ACS APPLIED MATERIALS & INTERFACES

Research Article

www.acsami.org

Physico-chemical Processes and Kinetics of Sunlight-Induced Hydrophobic ↔ Superhydrophilic Switching of Transparent N-Doped TiO_2 Thin Films

Madhusmita Sahoo,[†] Tom Mathews,*[,†] Rajini P Antony,[†] D. Nandagopala Krishna,[‡] S. Dash,[†] and A. K. Tyagi[†]

[†]Surface and Nanoscience Division, and [‡]Corrosion Science and Technology Division Indira Gandhi Centre for Atomic Research, Kalpakkam 603102, Tamil Nadu, India

Supporting Information

ABSTRACT: Sunlight-responsive anatase N-doped TiO_2 thin films undergoing reversible and switchable hydrophobic to superhydrophilic transition were synthesized by ultrasonic spray pyrolysis in a single step. Film thickness, roughness, surface morphology, crystal structure, composition, band gap, and wetting properties were studied using surface profilometry, scanning electron microscopy, X-ray diffraction, X-ray photoelectron spectroscopy, UV−vis spectroscopy, and water contact angle measurements, respectively. Surface X-ray photoelectron spectroscopy before and after sunlight irradiation revealed the major physicochemical process responsible for the hydrophobic → hydrophilic transition as surface hydroxylation and that responsible for hydrophilic → superhydrophilic transition as destruction of surface adsorbed organic species. The kinetic rates of the hydrophobic → superhydrophilic transition under sunlight and superhydrophilic → hydrophobic transition when kept under dark are found to be 0.215 min^{-1} and 2.03×10^{-4} min^{-1}, respectively.

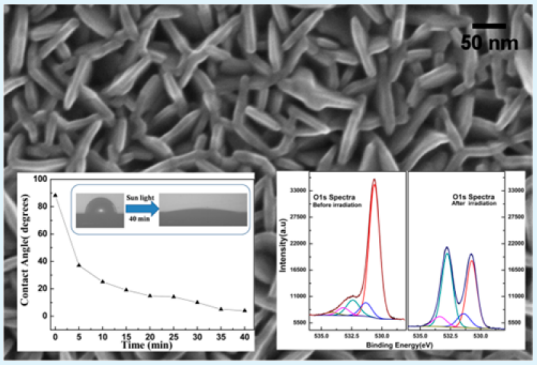

KEYWORDS: *N-doped TiO_2, thin films, photoinduced superhydrophilicity, hydrophobic−hydrophilic switching, switching mechanism, X-ray photoelectron spectroscopy*

INTRODUCTION

Nanocrystalline TiO_2 thin films and powders find application in photocatalytic destruction of organic wastes in air and water,[1,2] photocatalytic generation of hydrogen from water,[3] photovoltaic solar cells,[4,5] gas sensors,[6,7] self-cleaning surfaces.[8−12] The photoinduced hydrophobic ↔ superhydrophilic conversion of TiO_2 surfaces along with their ability to photo catalytically decompose organics have generated much interest in the past decade because of its potential use as self-cleaning surfaces.[13]The hydrophobic ↔ hydrophilic transitions of TiO_2 thin films were first reported by Wang and co-workers, who showed that under UV light irradiation, the wetting contact angle of polycrystalline TiO_2 thin films change from partially hydrophobic to superhydrophilic and revert to their initial hydrophobic state upon keeping under visible light or dark.[14] The commonly accepted physicochemical processes, responsible for the hydrophobic ↔ superhydrophilic switching behavior, though is in debate ever since Wang's report, are photoinduced reconstruction of TiO_2 surfaces due to hydroxylation[15] and removal of surface adsorbed organic species responsible for hydrophobicity.[16] When TiO_2 surface is irradiated with UV light, electrons from the valence band (VB) are excited to the conduction band (CB) leaving behind holes in the VB. The photogenerated electrons and holes "walk randomly" to the surface and holes attack the surface Ti−O bonds leading to their cleavage, resulting in formation of oxygen vacancies. These surface oxygen vacancies cause reduction of Ti^{4+} to Ti^{3+}, and the Ti^{3+} species facilitate dissociative chemisorption of molecular water at the oxygen vacancies leading to generation of surface hydroxyl groups. The generation of surface Ti−OH groups results in structural changes at the TiO_2 surface such that the intrinsically hydrophobic surface is converted to a hydrophilic one. The reverse happens, though slowly, when exposed to visible light/dark due to dehydration process and oxidation of Ti^{3+} to Ti^{4+}.[17] The second mechanism proposes migration of photogenerated holes and electrons to the surface followed by destruction of the very small amount of hydrocarbons, responsible for the hydrophobicity, present on the surface, by the reaction[16]

$$\text{hydrocarbons} + O_2 \rightarrow \text{oxidized products (such as } CO_2 \text{ and } H_2O)$$

Received: March 2, 2013
Accepted: April 16, 2013
Published: April 16, 2013

The reverse takes place by the recontamination of the hydrophilic surfaces by air-borne hydrophobic organics.[16] Presently, both the mechanisms are considered to be responsible for the reversible hydrophobic ↔ hydrophilic transition.

From the application point of view, control and reproducibility of the material properties is a basic prerequisite to improve its performance and reliability. The major drawback of TiO_2 is its wide band gap (~3:2 eV), which enables only about 5% of the solar spectrum, corresponding to the UV region (λ < 380 nm), to be absorbed. The visible region accounts for almost 45% of the solar spectrum. Hence, it is important to engineer the band gap of TiO_2 to make it a visible-light-absorbing material. Among the various methods adopted for making TiO_2 visible-light-absorbing, N-doping has been found to be energetically favorable and quite promising.[18] The wetting−dewetting properties of N-doped TiO_2 surfaces were studied by few groups in the recent past.[19−22] However, none of them report reversible hydrophobic ($\theta \geq 90°$) ↔ superhydrophilic ($\theta < 10°$) conversion in N-doped TiO_2 under sunlight/visible light. All the studies report reduction in contact angles in the hydrophilic regime ($\theta \approx 15-25°$) to ($\theta \approx 3-9°$)[19−21] and ($\theta \approx 80°$) to ($\theta \approx 55$ and $30°$).[22] A recent study by Wang et al.[23] on visible-light-driven reversible hydrophobic to hydrophilic transition of N-doped TiO_2 powders dispersed on a wafer surface reports water contact angle reduction from 135 ± 5° to 0° in 6 h of visible light irradiation. However, the authors did not report the results with respect to nature of N-doping. In all the reports on sunlight or visible-light-induced hydrophobic to hydrophilic conversion of N-doped TiO_2 surfaces, though the mechanisms have been proposed as reconstruction of TiO_2 surfaces due to hydroxylation and removal of surface adsorbed organic species responsible for hydrophobicity, experimental evidence for the increase in surface hydroxyl groups and decrease in carbon-containing surface species on photo irradiation are lacking. In addition to this, we have not come across any report on kinetics of reversible hydrophobic ($\theta \geq 90°$) ↔ superhydrophilic ($\theta < 10°$) conversion in N-doped TiO_2.

In the present study, we report synthesis of N-doped TiO_2 thin films by ultrasonic spray pyrolysis, a facile and very cost-effective open atmospheric technique, their hydrophobic ↔ superhydrophilic transition, kinetic rates of hydrophobic ↔ superhydrophilic conversion and surface XPS to understand the chemistry of the surfaces before and after photoirradiation and delineate the mechanism behind the reversible hydrophobic ↔ superhydrophilic transition. The kinetic rates of reversible hydrophobic ↔ superhydrophilic transitions are deduced following the theoretical analysis given by Seki and Tachiya.[24]

EXPERIMENTAL SECTION

Synthesis. Nitrogen-doped TiO_2 thin films were synthesized by ultrasonic spray pyrolysis technique described elsewhere.[25−27] For a typical synthesis, 50 mL of 0.035 M titanium oxyacetylacetonate and 20 mL of 0.15 M hexamine solution in alcohol was first ultrasonically atomized using a 1.7 MHz ultrasonic nebulizer. The generated aerosols, having fairly uniform size distribution in the range 0.5−5 mm with maximum distribution around 3 mm, were transported to the Si(100) substrates fastened on to a flat heater, through a vertical glass column. The substrate temperature was varied from 400 to 550 °C. The aerosols on reaching the hot zone evaporated and the vapors reacted with oxygen at the substrate surface to form the desired thin film.

Characterization. The film thickness and roughness were measured using a surface profilometer (Dektak, USA). The surface morphology of the thin films were analyzed using FESEM (Ziess, Germany) having EDAX facility. The crystal structure of the films were characterized by GIXRD (Bruker D8 Discover, Germany) using Cu Kα (λ = 1.5406 Å) radiation at 0.5° angle of incidence, with a scan step of 0.25° over 20−80°. The thin film surface chemistry before and after photoirradiation, as well as its chemical composition were studied using XPS (SPECS make, having monochromatic Al Kα radiation, at 1486.71 eV used as probe). The X-ray source was operated at a power of 300 W. Ar^+ ion beam with 1 keV and current of 0.5 mA was employed to sputter clean the specimen surface. An electron gun was used to neutralize charging during measurement. The spectrometer was calibrated using a standard silver sample. Data were processed by Specslab2 software. The BE of C-1s transition from contaminated C at 284.8 eV was used as a reference to account for any charging of the sample and the peak positions were compared to standard values for identification of different elements and their respective oxidation states. Optical absorption spectra of the thin films were recorded at room temperature using UV−visible spectrophotometer (AVANTES, The Netherlands)

Wetting studies. The water contact angle experiments were carried out by using a contact angle meter equipped with a CCD camera (Holmarc, HO-IAD-CAM-01, India). The contact angles were determined by analyzing the high resolution images of the water droplets on the thin films using ImageJ software. The as prepared samples were kept in the dark for a week and the water contact angles were measured. The contact angles of the samples, after exposure to sunlight of intensity ~10.0 mW cm^{-2}, were then measured as a function of exposure time. The samples were then kept under dark and the contact angles were measured intermittently in order to study the recovery of the initial hydrophobic state. The reversible and switchable wetting properties of the samples were studied by repeating photo irradiation, contact angle measurement followed by keeping in the dark and measuring the contact angle.

RESULTS AND DISCUSSION

The thickness and roughness of the films, synthesized at substrate temperatures of 400, 500, and 550 °C on Si(100) substrates, obtained from surface profilometry are given in Table 1. From the roughness values it is clear that the films are sufficiently smooth and coherent.

Table 1. Crystallite Size, Film Thickness, and Roughness of the N-Doped TiO_2 Films

synthesis temperature (°C)	crystallite size (nm)	film thickness (nm)	film roughness (nm)
400	19 ± 2	313	3.1
500	32 ± 3	297	2.9
550	54 ± 6	343	1.2

The microstructure of the films obtained from FESEM studies are given in Figure 1. The surface morphology of the films synthesized at 400 °C indicate the early stages of formation of grains. The surface is smooth and dense, but appears hazy. Well-defined grains could not be discerned. Formation of well-defined ~20 nm long and ~10 nm thick grains are easily discerned from the FESEM images of the samples synthesized at 500 °C. Because the film surface is very smooth and dense, the grain geometry in third dimension could not be discerned. The morphology of films synthesized at 550 °C show well-defined ~10 nm thick nanoplatelets with triangular and rectangular shapes. Crystal twinning can also be discerned.

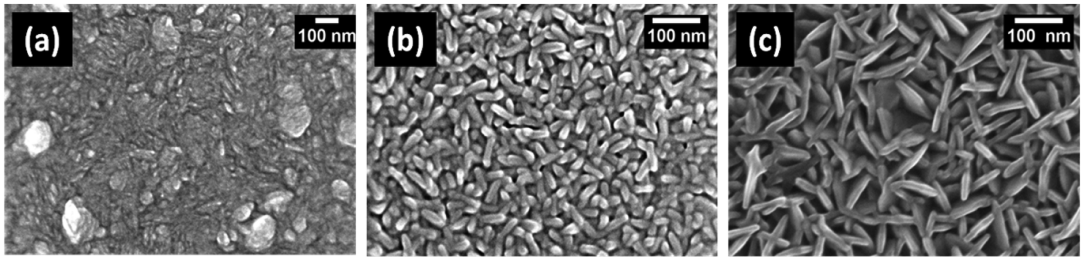

Figure 1. FESEM of N-doped TiO_2 synthesized at (a) 400, (b) 500, and (c) 550 °C.

The GIXRD patterns of pristine and N-doped TiO_2 thin films are shown in Figure 2. The films are of anatase phase, as

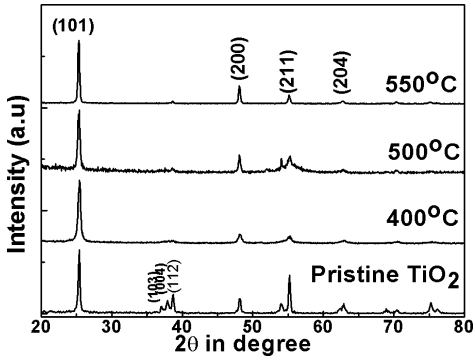

Figure 2. GIXRD pattern of pristine and N-doped TiO_2.

evidenced from the GIXRD patterns (JCPDS 21- 1272, space group I41/amd). The most intense peak appears at a 2θ value of 25.30°, which corresponds to the (101) plane of the anatase phase. The crystallite sizes calculated using Scherrer formula are given in Table 1. An increase in crystallite size with synthesis temperature is clearly seen. When the crystallites try to grow bigger in size with an increase in temperature, the film is expected to experience reduced magnitude of strain. The strain relaxation could have caused the morphological changes observed from the FESEM images, as strain relaxation can give rise to shape transition.[28]

X-ray photoelectron spectroscopic studies of the N-doped TiO_2 thin films were undertaken to understand the stoichiometry and bonding nature. The high resolution spectra were analyzed using the product of Gaussian and Lorentzian functions with the mixing parameter, "*m*" being 30% Lorentzian. For the background subtraction, conventional Shirley type fitting was used.

Typical N-1s spectra of the samples synthesized at 400 and 500 °C are shown in Figure 3. A similar pattern was obtained for films made at 550 °C. Depth profiling XPS was carried out to ascertain the nature and concentration of doped nitrogen at various depths. The N-1s spectra obtained at various sputter depths for films synthesized at 550 °C, given in Figure 1 of the Supporting Information, show same chemical nature and concentration of nitrogen at different depths indicating uniform distribution. The N-1s spectra all the samples were deconvoluted and found to consist of one high intensity peak at 396.6 eV and two low intensity peaks at 397.5 and 400.5 eV. In the case of samples synthesized at 500 °C, the broad deconvoluted peak at the tail end of the spectra was further deconvoluted to two peaks, 399.3 and 400.4 eV (Figure 2 in the Supporting Information). However, the χ^2 value obtained after

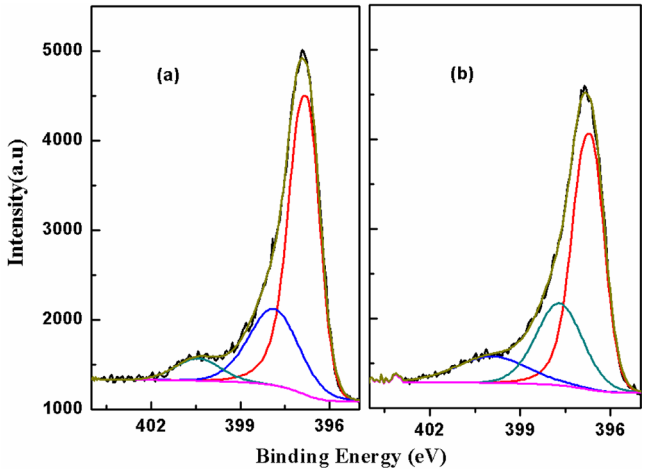

Figure 3. Deconvoluted N 1s spectrum of the N-doped TiO_2 synthesized at (a) 400 and (b) 500 °C.

the second deconvolution was not as good as before. The different N-1s BE values represent different electron density around nitrogen suggesting various N environments in the lattice. The high intensity peak at 396.6 eV and the low intensity peak at 397.5 eV can be ascribed to substitutional nitrogen (N_O) in the oxide lattice.[29−31] The variation of N-1s BE in the range 396−398 eV can be attributed to the variation in the number of N_O in each (TiO_6) octahedron. On the basis of the studies of Palgrave and co-workers[29−31] and Wang et al.,[32] the N-1s peaks in the range ∼399 to ∼401 eV can be assigned to interstitial nitrogen doping (N_i) at low levels in the presence of higher level N_O. The low peak intensity indicates a very low amount of N_i. Thus, the XPS data reveal incorporation of nitrogen to the TiO_2 crystal lattice mainly as N_O along with a very small amount of N_i.

The composition of the thin films synthesized at 400, 500, and 550 °C were calculated from the high resolution Ti-2p, O-1s, and the N-1s spectra, all obtained at 6 min sputter depth, using the equations

$$X_N = (I_{(N-1s)}/S_N)/[(I_{(Ti-2p)}/S_{Ti}) + (I_{(O-1s)}/S_O) + (I_{(N-1s)}/S_N)] \quad (1)$$

$$X_{Ti} = (I_{(Ti-2p)}/S_{Ti})/[(I_{(Ti-2p)}/S_{Ti}) + (I_{(O-1s)}/S_O) + (I_{(N-1s)}/S_N)] \quad (2)$$

$$X_O = (I_{(O-1s)}/S_O)/[(I_{(Ti-2p)}/S_{Ti}) + (I_{(O-1s)}/S_O) + (I_{(N-1s)}/S_N)] \quad (3)$$

dx.doi.org/10.1021/am400785x | ACS Appl. Mater. Interfaces 2013, 5, 3967−3974

and found to have 9.4, 8.0, and 2.6 at % of nitrogen, respectively, where $I_{N\text{-}1s}$ is the peak area of the N-1s peak corresponding to O−Ti−N (N_O), $I_{Ti\text{-}2p}$ is the sum of the areas of the Ti-2p deconvoluted peaks, and $I_{O\text{-}1s}$ is area of the O-1s corresponding to bonded oxygen. S_{Ti}, S_O, and S_N are sensitivity factors of the respective elements.

The optical band gap of the doped thin films are calculated using Tauc Plot (variation of $(\alpha h\nu)^{0.5}$ with $h\nu$), obtained from the absorption spectra of the samples. The Tauc expression is given as

$$(h\vartheta\alpha)^{1/n} = A(h\vartheta - E_g) \quad (4)$$

where h is the Planck's constant, ϑ frequency of vibration, α absorption coefficient, E_g band gap, and A the proportionality constant. The value of the exponent "n" denotes the type of transition. For direct allowed transition $n = 1/2$ and for indirect allowed transition $n = 2$. Because TiO_2 is an indirect band gap material, $n = 2$. The variation in $(\alpha h\nu)^{0.5}$ with $h\nu$, for samples synthesized at 400, 500, and 550 °C, are shown in Figure 4. It can be seen from the spectra that there are two linear regions. The optical band gap obtained by extending the major linear region to $x = 0$ was calculated as ~3.20 eV. The intercept from the smaller linear region show transition states situated at a difference of around 0.26 eV. This indicates introduction of interband state with substitutional N-doping. The first principle density-functional calculation by Lee et al.[33] have shown that absorption of visible light is due to isolated N-2p states above the valence band maximum of TiO_2 rather than band gap narrowing, as the mixing of N-2p states with O-2p states are too weak to produce significant band gap narrowing.[15,18,34] The additional features in the tail region of the spectra are due to the modified electronic structures although direct one to one correlation is not straightforward.[34]

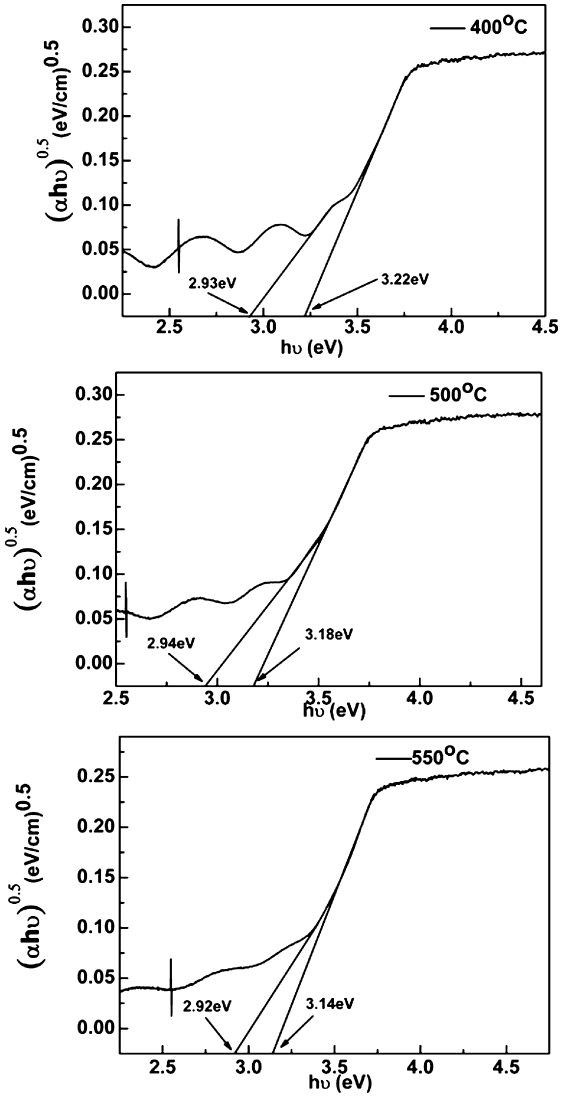

Figure 4. Tauc plot of N-doped TiO_2 thin films synthesized at 400, 500, and 550 °C.

The wetting characteristics of the N-doped samples were evaluated by contact angle measurements. All the samples exhibited hydrophobicity (contact angle in the range 88−105°) before light irradiation. The difference in the initial wetting contact angle (WCA) can be attributed to the difference in surface roughness. According to Cassie and Baxter[35,36] the WCA increases with roughness because of the cushioning effect from trapped air. The samples synthesized at 400 and 500 °C have roughness around 3 nm and have wetting contact angle around 105°. The sample synthesized at 550 °C has the least surface roughness (1.2 nm) and therefore has the lowest WCA (88°). Recently Boras and Gonzalez-Elipe[37] estimated the wetting contact angle for a smooth polycrystalline anatase−TiO_2 surface (free of OH-Ti), as 82°, from the results of wettability studies of polycrystalline anatase−TiO_2 films with different microstructure, texture and surface roughness using Miwa model.[38] The initial WCA of 88° for the sample having the least surface roughness (1.2 nm) is in reasonable agreement with the model value of 82°.

The variation in contact angle with duration of sunlight irradiation of ~10 mW cm^{-2} intensity, of the doped samples, is depicted in Figure 5. The sunlight intensity at the beginning, in between and end of irradiation was measured to ensure constant irradiation intensity. It can be seen from figure 5 that the doped samples synthesized at 500 and 550 °C attained superhydrophilicity upon exposure to sunlight for 40 min whereas the ones synthesized at 400 °C did not. No remarkable change in contact angle with sunlight irradiation could be seen in the case of pristine TiO_2 films synthesized at 550 °C, whereas the samples showed superhydrophilicity under UV light ($\lambda \approx 360$ nm). This indicates the visible-light-induced

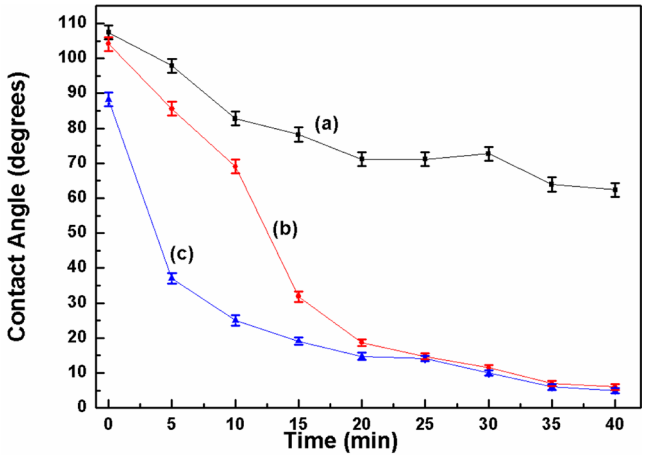

Figure 5. Variation in contact angle with irradiation time for samples synthesized at (a) 400, (b) 500, and (c) 550 °C.

dx.doi.org/10.1021/am400785x | ACS Appl. Mater. Interfaces 2013, 5, 3967−3974

hydrophobic → superhydrophilic conversion of N-doped TiO_2 films. The superhydrophilic N-doped samples synthesized at 550 °C when kept in dark for ∼5 days reverted to the initial hydrophobic state and on sunlight irradiation attained hydrophilicity in 30−40 min and reverted to hydrophobic state in 5 days confirming switching behavior (Figure 6).

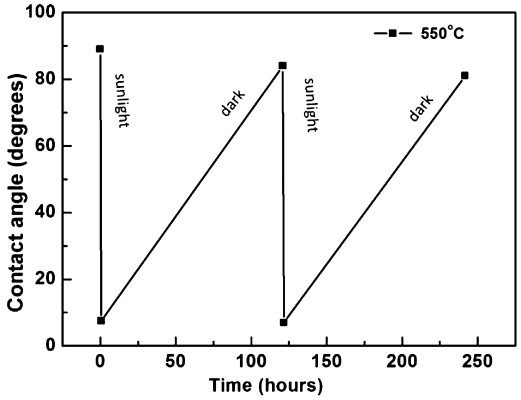

Figure 6. Switching pattern of N-doped samples synthesized at 550 °C.

Though all the samples are substitutionally N-doped, the sunlight driven hydrophobic → hydrophilic transitions are found to be different. To find the reason for the difference, we analyzed the thin film surfaces by XPS, before and after irradiation. The hydrophobic samples (before irradiation) were loaded into the XPS chamber under dark with its view ports covered with aluminum foils to avoid exposure to light during loading and analysis. Figures 7−9 shows the deconvoluted high

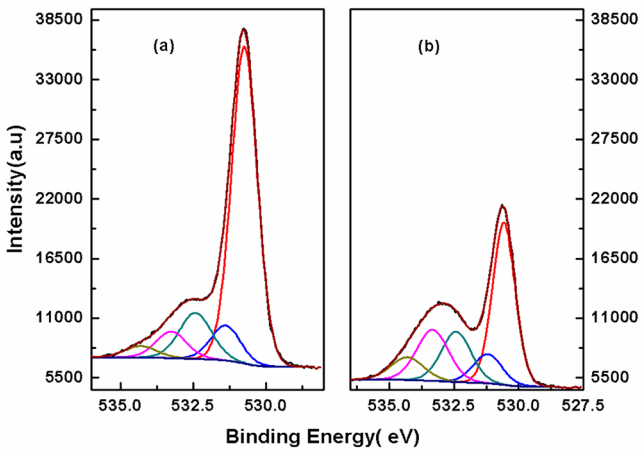

Figure 7. Deconvoluted O1s spectra of N-doped TiO_2 synthesized at 400 °C (a) before sunlight irradiation and (b) after sunlight irradiation.

resolution O-1s spectra of the films before and after irradiation. The O1s spectrum upon deconvolution shows five peaks. The peaks corresponding to BE values 530.6 and 531.3 eV can be attributed to the O−Ti bonds.[39,40] The peaks at 532.4 and 533.2 eV correspond to HO-Ti and adsorbed H_2O, respectively, and the one at 534.2 eV can be attributed to O−C bonds.[41−43] The fraction of HO-Ti species present can be evaluated from the area under the corresponding peak and relative sensitivity factor of oxygen, and is given in Table 2.

Table 2. Fraction of HO-Ti and CO Surface Species with Respect to Total Surface O−Ti

	OH/(Ti−O+OH)		CO/(TiO+OH+CO)	
synthesis temperature (°C)	before irradiation	after irradiation	before irradiation	after irradiation
400	0.139	0.247	0.0336	0.11
500	0.09	0.114	0.0186	0.0
550	0.113	0.447	0.0202	0.0

From the table, it is clear that for all the samples, the fraction of OH species bonded to Ti increases with sunlight irradiation confirming surface hydroxylation as one of the physicochemical process responsible for photoinduced hydrophilicity. Though there is an increase in HO-Ti species for films synthesized at 400 °C, superhydrophilicity was not observed. To understand the discrepancy, the O-1s peak at 534.2 eV attributed to O−C bonds were analyzed. The O−C bonds represent the presence of certain carbonaceous species at the film surface. From the area under the peak (Figure 7−9) and the relative sensitivity factors, the fraction/amount of the carbonaceous species (corresponding to the 534.2 eV O-1s peaks) present at the surface was evaluated. The calculated values are given in table-2. From Table 2, it is clear that there is no reduction in the amount of the carbonaceous species, in the case of samples synthesized at 400 °C, upon sunlight irradiation. This accounts for the observed hydrophobic → hydrophilic behavior of the samples. The samples did not attain superhydrophilicity upon sunlight irradiation. The analyses of 534.2 eV O-1s peaks, of samples synthesized at 500 and 550 °C, before and after sunlight irradiation clearly indicate destruction of the organic species represented by the 534.2 eV O-1s peak (Figures 8 and 9

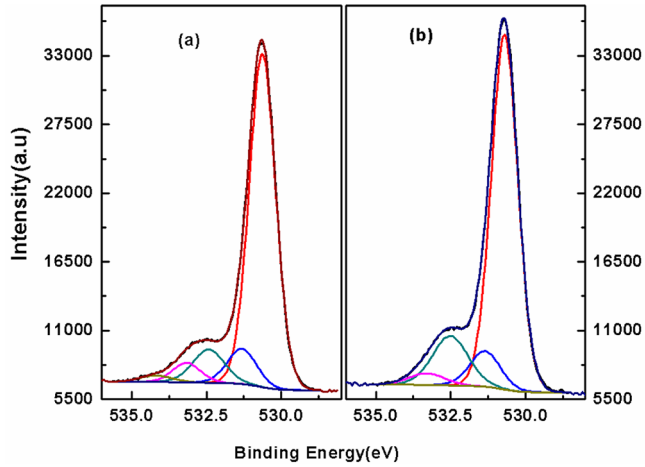

Figure 8. Deconvoluted O1s spectra of N-doped TiO_2 synthesized at 500 °C (a) before sunlight irradiation and (b) after sunlight irradiation.

and Table 2). These samples achieved superhydrophilicity upon sunlight irradiation (Figure 5) in 40 min. The results confirm the role of adsorbed carbonaceous species in the superhydrophilic behavior of TiO_2 surfaces. The reason for the presence of carbonaceous species, which account for the wetting performance of N-doped TiO_2 thin films synthesized at 400 °C, can be ascribed to the low synthesis temperature. The presence of carbon in the form of amorphous carbon as well as carbon containing compounds results from incomplete surface reaction of the carbon bearing metal−organic precursors used

dx.doi.org/10.1021/am400785x | ACS Appl. Mater. Interfaces 2013, 5, 3967−3974

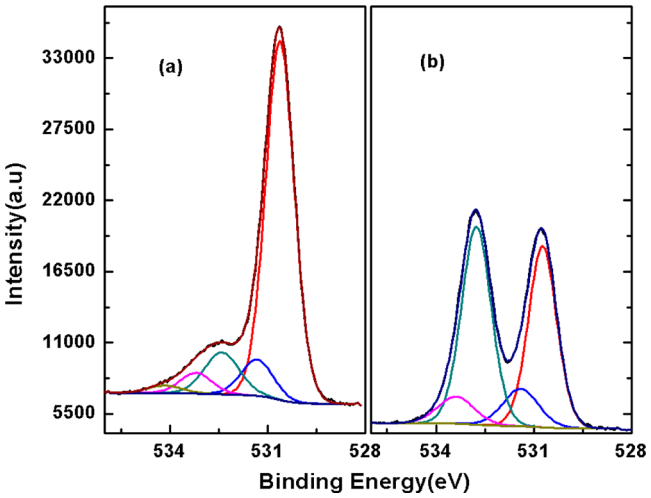

Figure 9. Deconvoluted O1s spectra of N-doped TiO_2 synthesized at 550 °C, (a) before sunlight irradiation and (b) after sunlight irradiation.

in the synthesis of N-doped TiO_2 films. The oxidation of the carbon/carbonaceous species present in the film matrix, to CO_2 and other gaseous products, increases with increase in temperature and is reflected as reduction in intensity of the corresponding C-1s peaks (Figures 3–5 in the Supporting Information). Similar trends were observed in previous studies.[26,27] A clear reduction in the intensity of peaks corresponding to BE values ~287.4 and ~289.75 eV, which correspond to oxygen bearing carbonaceous species, is seen in the case of samples synthesized at 500 and 550 °C, after sunlight irradiation, indicating the role of carbonaceous species in the superhydrophilic character of TiO_2 surfaces. No such reduction was observed in the case of films synthesized at 400 °C. This indicates that the major factor behind the hydrophobic → hydrophilic transition is surface hydroxylation whereas the process responsible for the hydrophilic → superhydrophilic transition is destruction of hydrocarbons present on the surface. In view of the above, the mechanism behind the hydrophobic → superhydrophilic conversion can be described as follows. The hydrophobic nature of the films indicates that its surface energy is not adequate to overcome the surface tension of water, when the water droplets come in contact with it. The low surface energy of the films can be attributed to the presence of adsorbed hydrocarbons. Because the molecular forces that hold the hydrocarbons together are much weaker than the forces that act between water molecules, the film surface do not possess adequate energy to overcome the water surface tension and consequently the surface remains hydrophobic. The photogenerated free electrons and holes diffuse to the surface and destroy the adsorbed hydrocarbon species generating high energy fresh surfaces. In addition, the holes attack and cleave the surface Ti–O bonds leading to the formation of surface hydroxyl groups and consequent surface restructuring enhancing the surface energy. The resultant high-energy surface decreases its energy by surface wetting. Thus the intrinsically hydrophobic surface is transformed to superhydrophilic.

The kinetic rates of hydrophobic ↔ superhydrophilic transition can be studied from the variation of cosine of contact angle ($\cos\theta$) with time. According to Young's theory the cos θ of a liquid droplet on a solid surface is a function of the interfacial energy between the solid and liquid[44] that in turn changes with the surface fraction of hydrophilic region. The three interfacial energies are related to the cos θ by the Young's equation

$$\gamma\cos\theta = \gamma_{SG} - \gamma_{SL} \quad (5)$$

where γ is the surface tension of liquid, γ_{SG} is the interfacial energy between the solid and the gas, and γ_{SL} is the interfacial energy between the solid and the liquid. Upon photoirradiation, the hydrophobic regions are converted to hydrophilic regions reducing the interfacial energy between the solid surface and liquid. Therefore, the change in fraction of hydrophilic region with time (rate of hydrophilic conversion during irradiation and the rate of hydrophobic conversion when kept in dark) can be represented as a function of cos θ. According to Seki and Tachiya[24] the difference in interfacial energy can be related to the surface fraction of hydrophilic region by the relation

$$f = \cos\theta = (\gamma_{SG} - \gamma_{SL})/\gamma = (\gamma_1(c) + \gamma_2)/\gamma = f_1 c + f_2 \quad (6)$$

where $f_1 = \gamma_1/\gamma$, $f_2 = \gamma_2/\gamma$, and c is the surface fraction of hydrophilic region. Assuming single rate constants for the photoassisted hydrophilic conversion and the hydrophilic to hydrophobic conversion under dark, they obtained the following rate equations

$$f_b(t) = \cos\theta = f_1 c_b(0)\exp(-k_b)t + f_2 \quad (7)$$

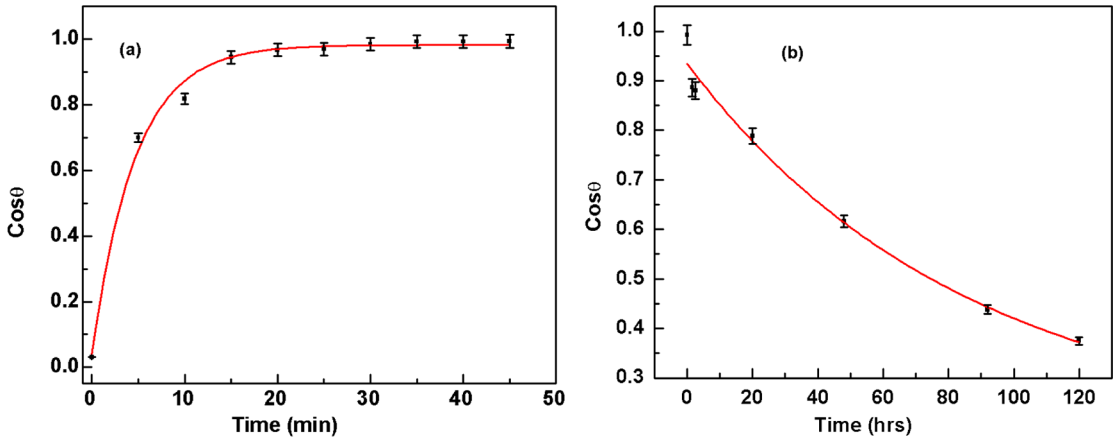

Figure 10. Variation in cos θ with time (a) under sunlight and (b) while being kept in the dark after the superhydrophilic surface is generated.

and

$$f(t) = \cos\theta = [f_1 c(0) - f_1 k_f/(k_f + k_b)]\exp -(k_f + k_b)t + [f_1 k_f/(k_f + k_b) + f_2] \quad (8)$$

for the hydrophilic to hydrophobic conversion under dark and photoassisted hydrophilic conversion respectively. Figure 10 depicts the variation in cos θ with time for the N-doped TiO_2 samples under sunlight irradiation as well as the respective decay in cos θ when kept in dark. The decay in cos θ in dark and increase in cos θ during photoirradiation with time are fitted using the exponential function given by eq 7 and 8, respectively. Reasonable agreement between equations and the experimental data can be seen for the forward and reverse processes. From the decay of cos θ with time kept in dark the rate of superhydrophilic → hydrophobic conversion is calculated as 1.97×10^{-4} min^{-1}. The long time ($t = \infty$) limit of cos θ obtained from eq 7 is the normalized interfacial energy of the hydrophobic surface, f_2, and is 0.1918 and it corresponds to the largest contact angle, 79°. The hydrophobic to superhydrophilic conversion rate, k_f, under sunlight can be obtained from the plot of cos θ against irradiation time, using the value of k_b. The calculated rate, k_f, is 0.216 min^{-1}. Because $k_f \gg k_b$, the largest value of cos θ obtained at $t = \infty$ from the cos θ versus time curve for the hydrophobic → superhydrophilic conversion can be described by cos $\theta = f_1 + f_2$. The highest value of cos θ corresponds to 0.99. The value of f_1 (which is γ_1/γ) obtained from the largest value of cos θ is 0.798. The smallest and largest contact angles obtained from the analysis of cos θ versus time curves given in panels a and b in Figure 10, 8 and 79°, respectively, matches with the corresponding experimentally observed values ∼5 and ∼88°.

CONCLUSION

Transparent N-doped TiO_2 thin films were synthesized by ultrasonic spray pyrolysis, a facile and very cost-effective open atmospheric technique, in a single step without any post-annealing/chemical treatment, which has the potential of scaling up. The incorporation of nitrogen into TiO_2 crystal lattice primarily as N_O along with very small amounts of N_i was confirmed from XPS studies. The N-doped samples were found to undergo hydrophobic → hydrophilic transition under sunlight irradiation. The hydrophilic samples reverted to the initial hydrophobic state in 5 days when kept in dark and became hydrophilic again on sunlight irradiation confirming the switching behavior. Analysis of the surface before and after irradiation, by XPS, revealed generation of HO-Ti species and destruction of organic species upon sunlight irradiation confirming the role of surface hydroxylation and organic species removal in the wetting behavior. The rate of hydrophobic → superhydrophilic conversion when irradiated with sunlight and the rate of superhydrophilic → hydrophobic conversion when the irradiated film is kept under dark calculated following the theoretical analysis of Seki and Tachiya is 0.22 min^{-1} and 2.03×10^{-4} min^{-1}, respectively. The N-doped TiO_2 films find application as transparent sunlight active antifogging coatings. The calculated kinetic rates help to fix the duration of photoirradiation for obtaining superhydrophilicity as well as decide how long the coating can be left in the dark without losing its superhydrophilicity.

ASSOCIATED CONTENT

Supporting Information

Figure 1 shows the representative N-1s spectra of the thin film synthesized at 550 °C at various sputter depths. Figure 2 shows the deconvoluted N-1s spectra of thin film synthesized at 500 °C. Figures 3, 4, and 5 show the C-1s spectra, before and after sunlight irradiation, of N-doped TiO_2 synthesized at 400, 500, and 550 °C, respectively. This material is available free of charge via the Internet at http://pubs.acs.org/.

AUTHOR INFORMATION

Corresponding Author

*E-mail: tom@igcar.gov.in.

Author Contributions

The manuscript is written through contributions of all authors. All authors have given approval to the final version of the manuscript.

Notes

The authors declare no competing financial interest.

ACKNOWLEDGMENTS

The authors acknowledge Dr. P. K. Ajikumar, Mr. Ashok Bahuguna, and Mr. Bonu Venkata Ramana, Surface and Nanoscience Division, IGCAR, Kalpakkam, for the FESEM, reflectance spectra, and surface profilometric measurements, respectively.

ABBREVIATIONS

WCA, water contact angle
XPS, X-ray photoelectron spectroscopy
GIXRD, glancing incidence X-ray diffraction
FESEM, field-emission scanning electron microscopy
CA, contact angle
BE, binding energy

REFERENCES

(1) Yu, J. C.; Ho, W.; Lin, J.; Yip, H.; Wong, P. K. *Environ. Sci. Technol.* **2003**, *37*, 2296−2301.
(2) Allain, E.; Besson, S.; Durand, C.; Moreau, M.; Gacoin, T.; Boilot, J. P. *Adv. Funct. Mater.* **2007**, *17*, 549−554.
(3) Antony, R. P.; Mathews, T.; Ramesh, C.; Murugesan, N.; Dasgupta, A.; Dhara, S.; Dash, S.; Tyagi, A. K. *Int. J. Hydrogen Energy* **2012**, *37*, 8268−76.
(4) Oregan, B.; Gratzel, M. *Nature* **1991**, *353*, 737−740.
(5) Nazeeruddin, M. K.; Kay, A.; Rodicio, I.; Humphry-Baker, R.; Mueller, E.; Liska, P.; Vlachopoulos, N.; Graetzel, M. *J. Am. Chem. Soc.* **1993**, *115*, 6382−6390.
(6) Lee, S. W.; Takahara, N.; Korposh, S.; Yang, D. H.; Toko, K.; Kunitake, T. *Anal. Chem.* **2010**, *82*, 2228.
(7) Iftimie, N.; Crisan, M.; Braileanu, A.; Crisan, D. C.; Nastuta, A.; Rusu, G. B.; Popa, P. D.; Mardare, D. *J. Optoelectron. Adv. Mater.* **2008**, *10*, 2363.
(8) Martinez-Ferrero, E.; Sakatani, Y.; Boissiere, C.; Grosso, D.; Fuertes, A.; Fraxedas, J.; Sanchez, C. *Adv. Funct. Mater.* **2007**, *17*, 3348.
(9) Bozzi, A.; Yuranova, T.; Guasaquillo, I.; Laubb, D.; Kiwi, J. *J. Photochem. Photobiol., A* **2005**, *174*, 156−164.
(10) Nakajima, A.; Hashimoto, K.; Watanabe, T.; Takai, K.; Yamauchi, G.; Fujishima, A. *Langmuir* **2000**, *16*, 7044.
(11) Fujishima, A.; Zhang, X. T.; Tryk, D. A. *Surf. Sci. Rep.* **2008**, *63*, 515.
(12) Parkin, I. P.; Palgrave, R. G. *J. Mater. Chem.* **2005**, *15*, 1689−1695.
(13) Carp, O.; Huisman, C. L.; Reller, A. *Prog. Solid State Chem.* **2004**, *32*, 33−177.

(14) Wang, R.; Hashimoto, K.; Fujishima, A. *Nature* **1997**, *388*, 431−432.
(15) Nakamura, R.; Tanaka, T.; Nakato, Y. *J. Phys. Chem. B* **2004**, *108*, 10617−10620.
(16) Zubkov, T.; Stahl, D.; Thompson, T. L.; Panayotov, D.; Diwald, O.; Yates, J. *J. Phys. Chem. B* **2005**, *109*, 15454−15462.
(17) Sakai, N.; Wang, R.; Fujishima, A.; Watanabe, T.; Hashimoto, K. *Langmuir* **1998**, *14*, 5918−5920.
(18) Asahi, R.; Morikawa, T.; Ohwaki, T.; Aoki, K.; Taga, Y. *Science* **2001**, *293*, 269−271.
(19) Yang, M. C.; Yang, T. S.; Wong, M. S. *Thin Solid Films* **2004**, *1-5*, 469−470.
(20) Yang, T. S.; Yang, M. C.; Shiu, C. B.; Chang, W. K.; Wong, M. S. *Appl. Surf. Sci.* **2006**, *252*, 3729−3736.
(21) Irie, H.; Washizuka, S.; Yoshino, N.; Hashimoto, K. *Chem. Commun.* **2003**, 1298−1299.
(22) Borras, A.; Lopez, C.; Rico, V.; Gracia, F.; et al. *J. Phys. Chem. C* **2007**, *111*, 1801−1808.
(23) Wang, J.; Mao, B.; Gole, J. L.; Burda, C. *Nanoscale* **2010**, *2*, 2257−2261.
(24) Seki, K.; Tachiya, M. *J. Phys. Chem. B* **2004**, *108* (15), 4806−4810.
(25) Raut, N. C.; Mathews, T.; Sundari, S. T.; Sairam, T. N.; Dash, S.; Tyagi, A. K. *J. Nanosci. Nanotechnol.* **2009**, *9*, 5298−5302.
(26) Raut, N. C; Mathews, T.; Ajikumar, P. K.; George, R. P.; Dash, S.; Tyagi, A. K. *RSC Adv.* **2012**, *2*, 10639−10647.
(27) Raut, N. C.; Mathews, T.; Panda, K.; Sundaravel, B.; Dash, S.; Tyagi, A. K. *RSC Adv.* **2012**, *2*, 812−815.
(28) Tersof, I.; Tromp, R. M. *Phys. Rev. Lett.* **1993**, *70*, 2782−2785.
(29) Palgrave, R. G.; Payne, D. J.; Egdell, R. G. *J. Mater. Chem.* **2009**, *19*, 8418−8425.
(30) Oropeza, F. E.; Harmer, J.; Egdell, R. G.; Palgrave, R. G. *Phys. Chem. Chem. Phys.* **2010**, *12*, 960−969.
(31) Takahashi, I.; Payne, D. J.; Palgrave, R. G.; Egdell, R. G. *Chem. Phys. Lett.* **2008**, *454*, 314−317.
(32) Wang, J.; Tafen, D. N.; Lewis, J. P.; Hong, Z.; Manivannan, A.; Zhi, M.; Li, M.; Wu, N. *J. Am. Chem. Soc.* **2009**, *131*, 12290−12297.
(33) Lee, J. Y.; Park, J.; Cho, J. H. *Appl. Phys. Lett.* **2005**, *87*, 11904.
(34) Xiaobo, C.; Burda, C. *J. Am. Chem. Soc.* **2008**, *130*, 5018−5019.
(35) Cassie, A. B. D.; Baxter, S. *Trans. Faraday Soc.* **1944**, *40*, 546−551.
(36) Feng, X.; Zhai, J.; Jiang, L. *Angew. Chem., Int. Ed.* **2005**, *44* (32), 5115−5118.
(37) Borras, A.; González-Elipe, A. R. *Langmuir* **2010**, *26* (20), 15875−15882.
(38) Miwa, M.; Nakajima, A.; Fujishima, A.; Hashimoto, K.; Watanabe, T. *Langmuir* **2000**, *16*, 5754.
(39) Ingo, G. M.; Dire, S.; Babonneau, F. *Appl. Surf. Sci.* **1993**, *70−71*, 230.
(40) Kuznetsov, M. V.; Zhuravlev, J. F.; Gubanov, V. A. *J. Electron Spectrosc. Relat. Phenom.* **1992**, *58*, 169.
(41) Pouilleau, J.; Devilliers, D.; Groult, H.; Marcus, P. *J. Mater. Sci.* **1998**, *32*, 5645.
(42) Nefedov, V. I.; Gati, D.; Dzhurinskii, B. F.; Sergushin, N. P.; Salyn, Y. V. *Zh. Neorg. Khim.* **1975**, *20*, 2307.
(43) Glenis, S.; Benz, M.; LeGoff, E.; Schindler, J. L.; Kannewur, C. R.; Kanatzidis, M. G. *J. Am. Chem. Soc.* **1993**, *115*, 12519−12525.
(44) Young, T. *Phios. Trans. R. Soc. London, Ser. A* **1805**, *95*, 65−87.